PAPER

Optically active quadrupole edge modes in arrays of flat metallic nanodisks

To cite this article: Seyed M Sadeghi et al 2021 J. Opt. 23 025003

View the <u>article online</u> for updates and enhancements.



IOP ebooks™

Bringing together innovative digital publishing with leading authors from the global scientific community.

Start exploring the collection-download the first chapter of every title for free.

IOP Publishing Journal of Optics

J. Opt. 23 (2021) 025003 (7pp)

https://doi.org/10.1088/2040-8986/abe451

Optically active quadrupole edge modes in arrays of flat metallic nanodisks

Seyed M Sadeghi^{1,*}, Waylin J Wing² and Rithvik R Gutha³

- ¹ Department of Physics and Astronomy, University of Alabama in Huntsville, Huntsville, AL 35899, United States of America
- ² EOTECH, 1201 E. Ellsworth Rd, Ann Arbor, MI 48108, United States of America
- ³ Department of Physics and Astronomy, Living Systems Institute, University of Exeter, Exeter EX4 4QD, United Kingdom

E-mail: seyed.sadeghi@uah.edu

Received 2 December 2020, revised 15 January 2021 Accepted for publication 8 February 2021 Published 19 March 2021



Abstract

Using experimental and simulation methods, we demonstrate that structures consisting of two-dimensional arrays of closely-packed flat metallic nanodisks can support optically active collective resonances associated with the dark edge modes. Our results show that such resonances appear as the refractive index of the superstrate increases, generating a relatively sharp peak with weak sensitivity to the variations of the environment. Using a consecutive multilayer deposition of Si on the top of the arrays we map the development of such a resonance via multi-step red shifting of the Rayleigh anomaly wavelength. The results show that when the Rayleigh wavelength is sufficiently close to the subradiant quadrupole edge modes of the nanodisks, a linearly polarized light can excite such modes, resulting in optically active collective resonance.

Keywords: sub-radiant edge modes, dark modes, Rayeligh anomaly, surface lattice resonances, nanodisks, optical activation

(Some figures may appear in colour only in the online journal)

1. Introduction

The interaction of metallic nanostructures with light is a broad subject of research with a wide range of applications. Amongst these, nanostructures that support visible and infrared plasmonic features are extensively studied for optical filters, lasers, sensors, polarization devices, etc [1–5]. The interaction of light with metallic nanostructures is overwhelmingly involved with their optically active plasmonic resonances, such as their dipoles. Higher-order dark resonances, such as quadrupole modes, can couple to an incident electromagnetic field when the symmetries of the structures are broken and mixing between otherwise subradiant multipolar modes with the bright dipolar modes occurs [6]. Subradiant modes can also become bright using phase retardation [7], electromagnetically induced transparency [8], and vortex beams with specific

angular momentum [9]. Recent theoretical studies show that quadrupole lattice resonances in square lattice plasmonic crystals composed of nanodisks can be excited by vertically incident cylindrical vector beams [10]. The coupling of subradiant plasmonic modes with lattice modes of periodic arrays of metallic nanoparticles has also been investigated recently [11, 12]. A recent report has shown that the inter-nanoantenna plasmonic coupling in arrays of metallic nanoantennas allows the forbidden quadrupole states of the nanoantennas to become the dominant visible optical features of the arrays [13].

Most of these investigations have been carried out in nanostructures that support multipolar localized surface plasmon resonances. It is known, however, that when the lateral dimensions of metallic nanostructures are much larger than their heights, forming flat metallic nanoantennas, their plasmonic resonances fall into two categories, i.e. edge and cavity modes [14–17]. The edge modes happen at the edges of the nanostructures and can have various multipolar characteristics. On

^{*} Author to whom any correspondence should be addressed.

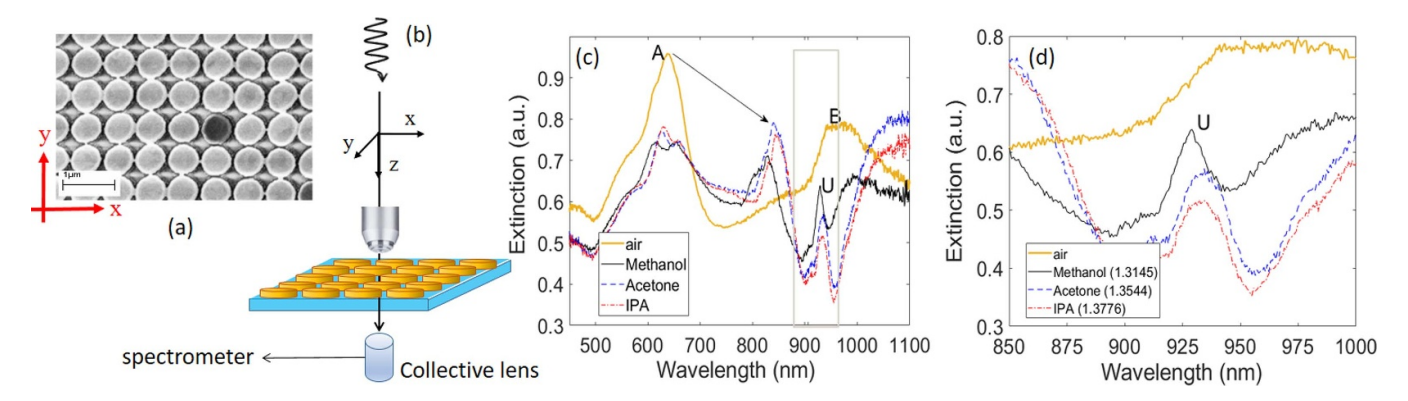


Figure 1. (a) Top view of the SEM image of the closely packed FNDs (sample A). (b) Transmission optical setup used to measure extinction spectra of the structures. (c) The extinction spectra of the structure when the superstrate is air (thick solid line), methanol (thin solid line), acetone (dashed line), and IPA (dotted-dashed line). (d) A close-view presentation of the results in (c). The numbers in parentheses in the legends of (c) refer to the refractive index of the chemicals.

the other hand, the cavity, or breathing modes, are formed at the center of the nanostructures [14, 18]. Recently, coupling of the edge modes in dimers planar nanostructures has been addressed, demonstrating the possibility of bonding and antibonding modes [16]. Additionally, the optical properties of arrays of flat metallic nanoantennas have shown the possibility of hybridization of the edge modes with the Rayleigh anomaly, forming surface lattice resonances (SLRs) [5, 19, 20]. Recent reports have also investigated the impact of flat metallic nanoantennas on dynamics of excitons in semiconductor quantum dots biologically adsorbed to such nanoantennas, [21, 22] and the formation of super-plasmonic cavities in closely-packed flat metallic nanoantennas [23]. Extensive research has also been devoted to plasmonic properties of nanoplates with different shapes, including triangular [24, 25], fractal shapes [26, 27], and flat metallic nanoantennas made with different materials [28, 29].

In this paper we use experimental and simulation techniques to study lattice-induced plasmonic-photonic activation of dark edge modes of Au flat nanodisks (FNDs). For this, we consider structures consisting of closely-packed twodimensional arrays of such FNDs (figure 1(a)). We demonstrate that when such a structure is excited with a linearly polarized light, the increase in the refractive index of the superstrate allows the formation and amplification of a collective resonance with relatively narrow optical features in the near infrared range. Our results show that such a resonance is the result of orthogonal coupling of the subradiant quadrupole edge modes with the neighboring FNDs via lattice plasmonic and photonic couplings. We use consecutive deposition of Si layers on the top of the FND array to map formation of the collective resonance involving with such modes. This technique allows us to shift the Rayleigh anomaly wavelength step-bystep closer to those of the dark quadrupole modes of the FNDs until the coupling process is established efficiently. Simulation results are used to study the mode profiles of such a resonance.

Note that we previously reported that in arrays of long flat metallic nanoantennas edge mode coupling can form a superplasmonic cavity resonance characterized by anomalously high order standing waves in each nanoantenna [23]. Such a process can lead to the formation of supercells that transform the two-dimensional arrays of such nanoantennas into a one-dimensional array, wherein such supercells are periodically repeated [30]. The edge-mode coupling studied in this paper, however, does not stimulate any higher order plasmonic modes, rather it involves the intrinsic dark quadrupole of the FNDs.

2. Experimental and numerical methods

Samples included arrays of FNDs with square structural lattices, fabricated onto a micro cover glass substrate using ebeam lithography. In sample A the FNDs have diameters of about 560 nm and the lattice constants of arrays (a_x and a_y) are both 600 nm. This leaves about 40 nm for the edge-to-edge spacing between the FNDs along the x and y axes (figure 1(a)). We also fabricated another sample (sample B) wherein the diameter of the FNDs were about 650 nm but $a_x = a_y = 1000$ nm. The extinction spectra were measured using a transmission setup consisting of a halogen lamp, polarizer, microscopic objective, and collective lens. Samples were placed between the objective and the collective lens which directed part of the transmitted light toward a sensitive spectrometer (Ocean Optics TE cooled QE-Pro) using fiber optics. The collective lens was placed at sufficient distance right beneath the microscope objective to ensure a well-defined and small angle spread of illumination (figure 1(b)). To study how the optical responses of these structures were changed with refractive index we used droplets of acetone, isopropyl alcohol (IPA), or methanol on the top of the arrays. The refractive indices of these organic liquids are 1.3544, 1.3771, and 1.3145, respectively. We also studied the extinction spectra of sample A while ultrathin layers of amorphous Si were sputtered on the top of the FNDs. This allowed us to map the evolution of the extinction spectra of the sample as the refractive index of the superstrate was gradually increased. To carry out numerical simulations we used the finite-difference time-domain technique provided by the Device Multiphysics Simulation Suite of Lumerical (2020a).

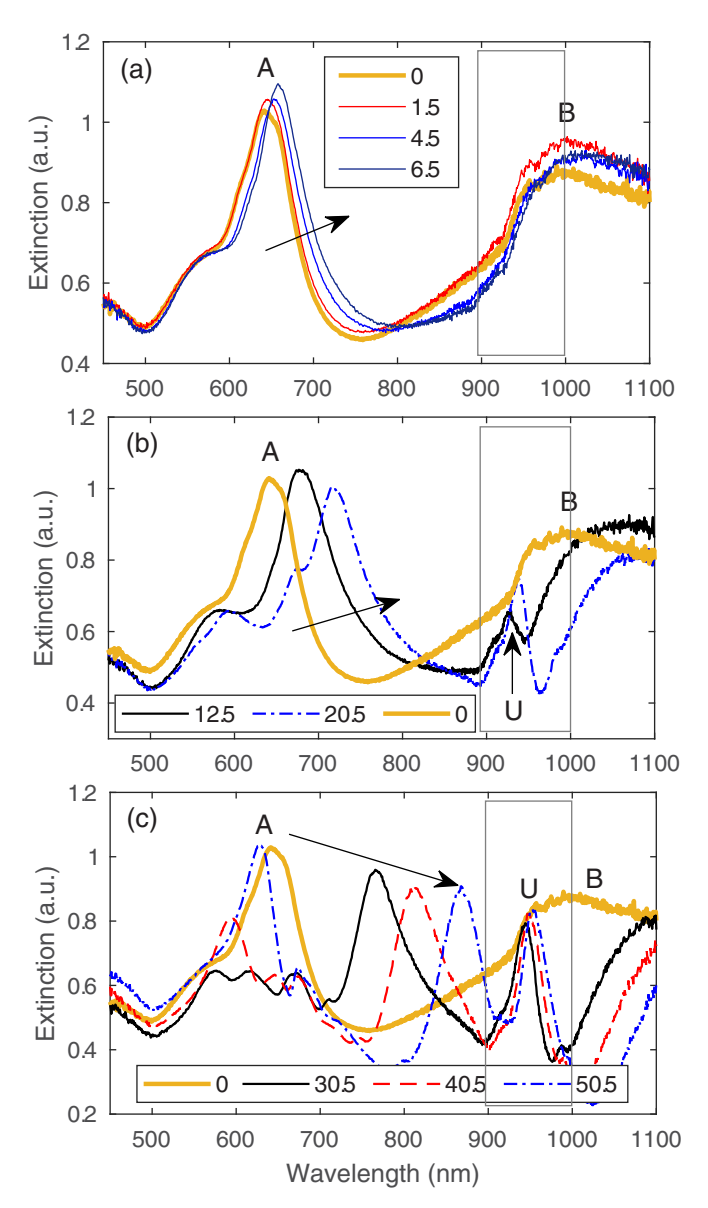


Figure 2. Variations of the extinction spectra of sample A for different thicknesses of Si layer, d (legends). (a) Evolution of the spectrum from d=0 to 6.5 nm, (b) from d=12.5 to 20.5, and (c) from d=30.5 to 50.5 nm.

3. Optics of closely packed FNDs

The results shown in figure 1(c) demonstrate the extinction spectrum of sample A when the superstrate is air (thick solid line), methanol (solid line), acetone (dashed line), and IPA (dotted-dashed line). For the case of air, the results show that this sample supports two main peaks; peak A at \sim 640 nm, peak B at 950 nm. As shown in figure 1(c), adding methanol, acetone, and IPA leads to a significant shift of peak A (arrow). This figure shows that the wavelength shifts of peak A follows the refractive indices of the chemicals, suggesting a high sensitivity to the variations of the refractive index of the environment (about 325 RIU nm $^{-1}$ wherein RIU refers to refractive index unit). Similar features were also observed for smaller FNDs, as reported in [31, 32]. A unique feature of the results

shown in figure 1(c) is, however, the formation of a sharp peak (peak U) at about 930 when the chemicals are added (highlighted with a rectangle). Figure 1(d) shows the details of variations of the extinction spectra of the FND array around the wavelength range where peak U is generated.

To study the details of the evolution of peak U, we sputtered several layers of amorphous Si on the top of FNDs. After each layer we measured the extinction spectra of the arrays. The results presented in figure 2(a) show the spectra when the thickness of the Si layer (d) was increased with an interval of about 1 nm, up to 6.5 nm. These results show that peak A demonstrates well-resolved red shifts. However, no significant feature that indicates the formation of peak U can be seen here. Crucial to note here is that the thickness of the layers was up to 6.5 nm; since the thicknesses of the sputtered Si layers were small, they were basically converted to Si oxide after exposure to air. Considering this, the results in figure 2(a) highlight the high refractive index sensitivity of the FND arrays.

Figure 2(b) shows variations of the extinction spectra as d increases from 12.5 to 20.5 nm. The results demonstrate that peak A undergoes further red shift up to about 100 nm. Under these conditions peak U starts to appear around 925 nm. As d increases further this peak becomes more prominent (figure 2(c)). When d = 50.5 nm, peak A shifts by about 250 nm while peak U continues to become stronger and red shifted to some extent. Figure 3 shows the details of the evolution of peak U for d = 0 up to 50.5 nm and figure 4 compares the wavelength shifts of peaks A (circles) and U (squares) as a function of d. Note that a distinct feature of peak A seen in figure 2 is that, although it is red shifted significantly, its spectral width does not increase. This feature makes this peak an appealing host for the investigation of sensors with high refractive index sensitivity and figure of merit [31]. Note that the results in figure 2 show the detailed evolution of the peak A as the refractive index of the superstrate increases. As seen in figures 2(b) and (c), this process is involved with the formation of some peaks at the wavelength range of peak A when the superstrate was air. This process is repeated, although to a lesser extent, in figure 1(c). The induced extra peaks seem to be the result of enhancement and shift of the mode associated with a hump seen in the shorter wavelength side of peak A in figure 2(a).

Figure 5(a) shows the results for sample B with the lattice constants of 1 μ m (inset). In this case we see that the FNDs are spaced much farther apart than those seen in sample A. The results in the absence of the chemicals show a dominant peak at about 1050 nm (line 1). The addition of the chemical pushes this peak beyond the spectrometer range. Here, however, we do not see any features similar to peak A or peak U seen in the case of sample A. Additionally, the results for acetone (line 2), methanol (line 3) and IPA (line 4) in figure 5(a) suggest the formation of peaks in the visible range. To see this clearly, in figure 5(b) we show a close view of the spectra in the range 500–900 nm. These results show that the addition of each chemical generates two peaks with high sensitivities to the refractive index of the superstrate.

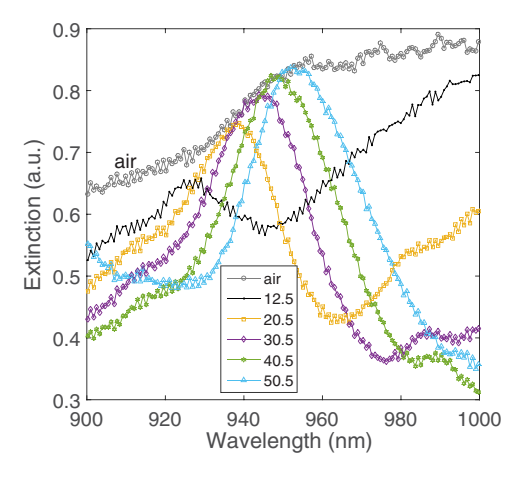


Figure 3. Details of variations of peak U with thickness of the nominal thickness of the sputtered Si layers (legends in nm).

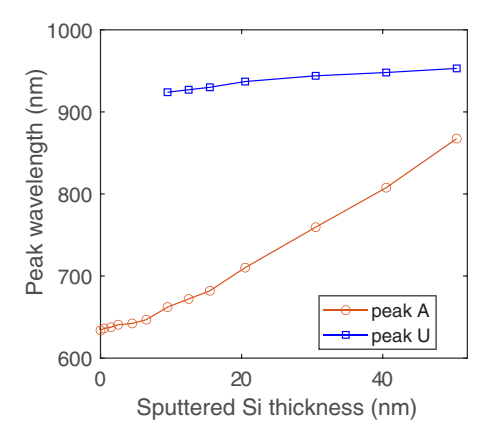


Figure 4. Variation of the peak wavelength of peak A (circles) and peak U (squares) as a function of the thickness of the sputtered Si layer.

The doubling seen in figure 5(b) can be associated with the variation of the shapes of FNDs in sample B and possibly the formation of a second order SLR. For the latter, note that for the incident light perpendicular to the array's plane, the Rayleigh anomaly wavelength, can be found using $\lambda_{RA} = n_{\sup} a_x / m$. Here n_{\sup} is the refractive index of the superstrate, mth is the order of diffraction, and a_x is the lattice constant along the x-axis. For the case of sample B $a_x = 1000$ nm. Therefore, considering m = 2, λ_{RA} becomes about 650 nm when the chemical was added. For this case of the first order diffraction (m = 1) λ_{RA} falls around 1.3 μ m. On the other hand, for the case of peak A of sample A, when the superstrate is air for the first order diffraction, $m=1, \lambda_{RA}=600$ nm. Therefore, as discussed in [32], this peak can be associated with the SLR caused by the hybridization of the plasmon resonances of the FNDs with the Rayleigh anomaly. As the effective refractive index of the superstrate increases, by adding Si layers, λ_{RA} is also red shifted. In the presence of the chemical λ_{RA} becomes about 750 nm, which is fairly close to the peak (figure 1(c)) [32].

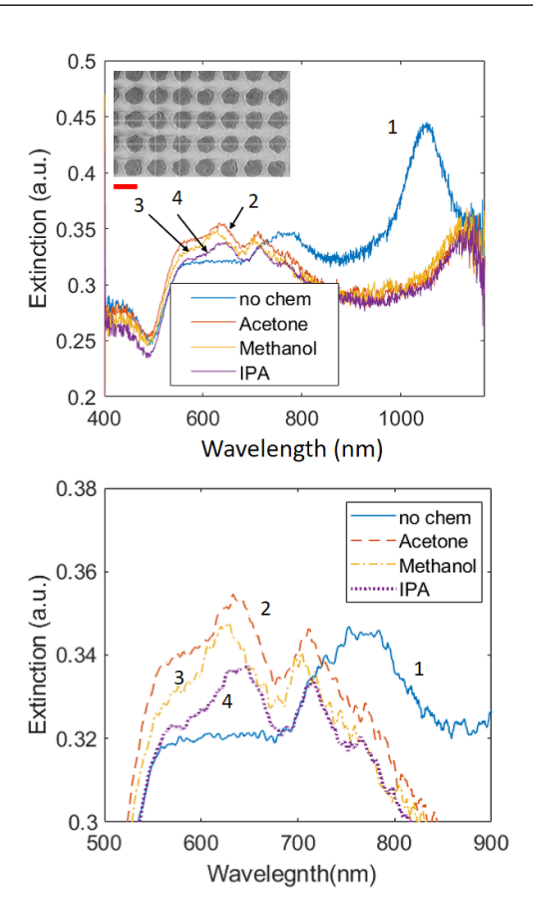


Figure 5. (a) Extinction spectra of sample B in the absence of the chemical (line 1), and in the presence of the acetone (line 2), methanol (line 3), and IPA (line 4). The scale bar in the inset is 1 μ m. (b) shows a close view of the spectra in the 500–900 nm range.

4. Lattice quadrupole edge modes

Multipolar edge modes in flat nanosquares have been studied before [14]. Similar to the case studied in this paper, it has been shown that quadrupole modes of such structures, which are concentrated at their edges, are mostly dark. As a result, they do not show up in the optical spectrum. Previous reports have used electron loss energy spectroscopy to study these modes [14, 15, 17]. Such a technique has also been used to study the coupling of higher order plasmonic resonances, leading to bonding and anti-bonding edge mode coupling [16]. The key aspect of the current paper is the demonstration of the optical activation of quadrupole edge modes via their photonic-plasmonic coupling in an array of FNDs.

To discuss the mechanism behind peak U and its relation with edge modes of the FNDs, we carried out a simulation to study the modal field properties of sample A. Figure 6(a) shows the simulation structure with similar specifications to those of sample A. Here we assumed the incident light reaches the structure along the z-axis and it is polarized along the x-axis. We also considered the mesh size of 3 nm while defining a unit cell consisting of a single FND with periodic boundary conditions in the x-y plane. The planar incident light source reached this unit from the top while a monitor was

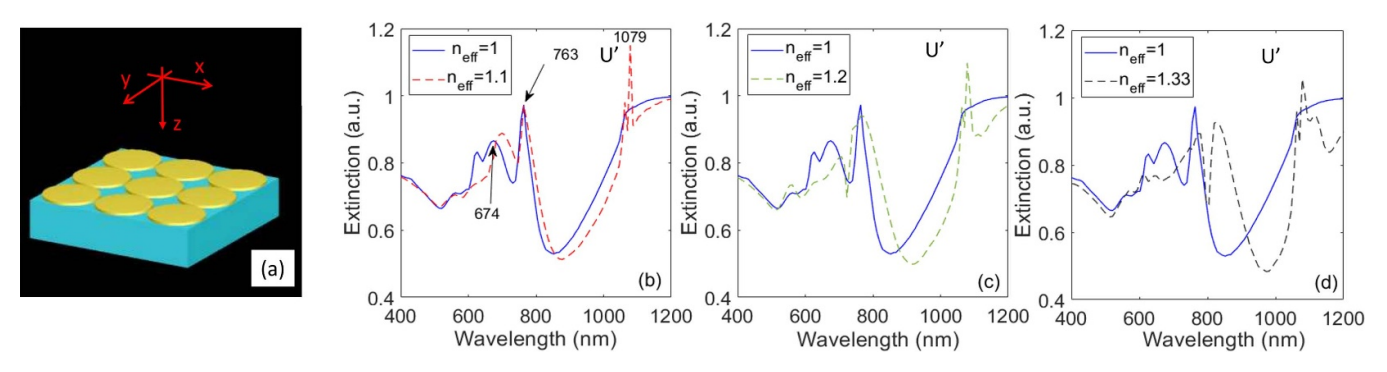


Figure 6. (a) Simulation structure of sample A. (b)–(d) Extinction spectra when the effective refractive index of the superstrate is 1.1, 1.2, and 1.33 (dashed lines), respectively. The solid lines refer to the extinction spectrum when the superstrate is air ($n_{\text{eff}} = 1$).

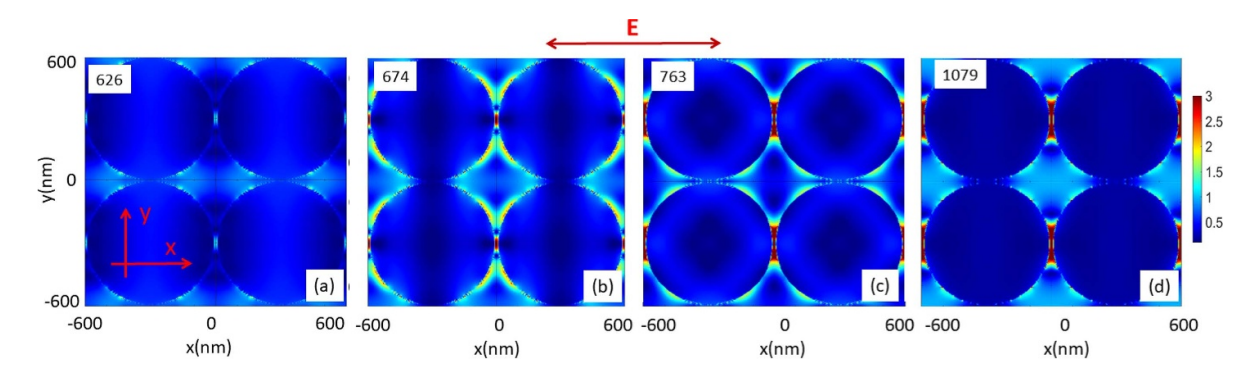


Figure 7. Enhancement field mode profiles at 626 (a), 674 (b), 763 (c) and 1079 nm (d) when the effective refractive index of the superstrate is 1 (air).

placed at the other side to obtain its transmittance (T). Having T, the extinction was obtained using 1-T.

The solid lines in figures 6(b)–(d) show the results for the extinction spectrum of such a structure when the superstrate was air. The spectrum matches fairly well with the experimental results in figure 2 (thick solid line). In the range of 900-1200, in particular, we see a broad feature without any feature associated with peak U. In addition to this, we also see two peaks, one at 674 nm and the other at 763 nm. When the effective refractive index of the superstrate $(n_{\rm eff})$ becomes 1.1 (red dashed line), a sharp peak (U') is formed at 1079 nm (figure 6(b)). The higher refractive index sensitivity of the 674 nm peak can be associated with the coupling of plasmonic edge modes at this wavelength with the photonic modes in the superstrate [20, 32]. As the refractive index of the superstrate increases further, as shown in figures 6(c) and (d), peak U' does not shift while the rest of the plasmonic features are red shifted (dashed lines).

To study the mode properties of the results shown in figure 6, we first consider the case when the superstrate is air (solid lines). Figure 7 shows the results for the field enhancement mode profiles in the x-y plane associated with this case at 626 (a), 676 (b), 763 (c) and 1079 nm (d). In (a) we can see some weak residual of the field coupling the FNDs along the y-axis. In the case (b), in addition to some plasmonic edge coupling along the x-axis, the FNDs are coupled to each other via higher order modes along the same axis. At 763 nm, the results in figure 7(c) suggest a dominant direct plasmonic edge

mode coupling. Some features of the edge mode quadrupole can also be seen. These modes, however, are not coupled to the neighboring FNDs. At 1079 nm (figure 7(d)) similar features, such as those seen in figure 7(c), occur. Here, however, some weak cross-coupling between FNDs can also be seen [20].

Figure 8 shows the mode field enhancement profiles of the three main peaks seen in figure 6(b) (red dashed line), i.e. for the case when $n_{\text{eff}} = 1.1$. Figures 8(a) and (b) show the profiles associated with the peaks at 698 and 763 nm, respectively. The 698 nm peak is associated with the 674 nm peak in figure 6(b), after about 24 nm red shift. Note that this peak supports a weak multipolar coupling along the x-axis. Such a process does not happen for the case of the 763 nm peak (figure 8(b)). Rather, in this case, we see a stronger near-field plasmonic coupling. The results in figure 8(c) suggests that the sharp peak U' is associated with a well-established lattice coupling of the edge mode quadrupoles. Along the x-axis (polarization axis of the incident light), the plasmonic fields of the neighboring FNDs are efficiently coupled to each other, similar to the case shown in figure 7(d). Along the y-axis, however, we can see photonicplasmonic coupling of the quadrupole edge modes. At a similar wavelength range, when $n_{\text{eff}} = 1$ (figure 7(d)), such edge modes are hardly excited.

The results shown in figure 8(c) suggest that sample A can support a unique plasmonic-photonic lattice, wherein along the *x*-axis the plasmonic near fields at the edges of the FNDs are efficiently coupled to each other. Along the *y*-axis, however, the quadrupole edge modes are coupled via hybridization

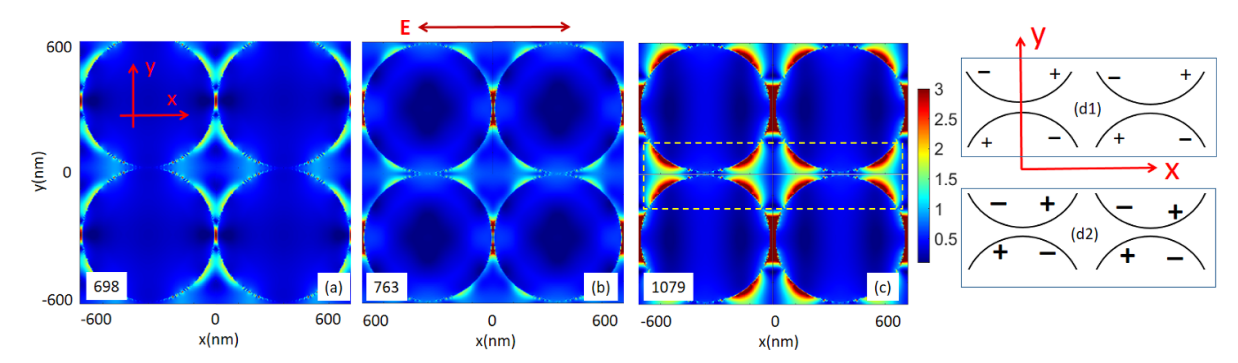


Figure 8. Enhancement field mode profiles when the effective refractive index of the superstrate is 1.1 at 698 (a), 763 (b) and 1079 nm (c). Schematic illustration of charge distribution at the region highlighted with dashed rectangles in (c) when the refractive index of the superstrate is 1 (d1) and higher (d2).

with the Rayleigh anomaly, becoming optically active. To see this, note that the results presented in figure 2 show how the step-by-step shift of λ_{RA} can impact the formation of peak U. As layers of the Si were deposited, this wavelength was red shifted. Figure 2(b) suggests that the initial appearance of peak U occurs when d = 12.5 nm. Bearing in mind that the thicknesses of the Si layers were small, because of oxidation, we consider their refractive indices to be close to that of silica, i.e, \sim 1.45. Assuming the range of the plasmonic field of FNDs in a superstrate is typically about 50 nm, this suggests that for d = 12.5 nm $n_{\rm eff}$ can be about 1.1. This put the value of λ_{RA} at around 660 nm. This trend continues as d increases. For d =50.5 nm, the whole plasmon mode volume is likely to be filled with a mixture of Si and Si oxide. This pushes λ_{RA} to about the 900 nm range. Such an understanding seems to be consistent with the results in figure 4 (squares).

The results presented above demonstrate the profound impact of the refractive index of the superstrate in the formation of the quadrupole edge-mode coupling. This can be related to the fact that the addition of the chemical or the Si layers allows the medium to become more homogeneous. Under this condition, the plasmonic modes of the FNDs are enhanced and the coupling process becomes stronger. In fact, when the superstrate is air the charge distribution associated with the quadrupole edge modes supports relatively low concentration, as schematically shown in figure 8(d1). When the refractive index of the superstrate increases, the charge accumulation is enhanced, while they are more concentrated close to the y-axis (figure 8(d2)) [33–35]. This process is similar to the case of dimers consisting of flat-gap antennas when their transverse modes are excited [33]. A key issue here, however, is that the increase in refractive index leads to the red shift of λ_{RA} , allowing hybridization of the edge modes with Rayleigh anomaly.

Note also that, in contrast to the two-dimensional arrays of long metallic nanoantennas studied in [23, 30], the FNDs studied here have radial symmetry in the *x*–*y* plane. This made their optical responses similar whether the incident light polarization was along the *x*-axis or the *y*-axis. Therefore, while for the case of long metallic nanoantenna arrays, the anti-bonding edge mode coupling occurred only for transverse polarization [30], here it happens for both states of polarization. Additionally, as seen in figure 8(c), in the case of FND arrays the

optically activated edge modes are associated with the intrinsic dark quadrupole modes of the FNDs. In the case of long flat nanoantennas, however, edge mode coupling happens with the generation of anomalously high order plasmonic standing waves along the nanoantennas, forming one-dimensional supercells [23, 30].

5. Conclusions

We studied the optical activation of dark edge modes of flat Au nanodisks. The results showed that when such nanodisks were formed in periodic form and they were closely packed together such that their edge-to-edge spacings were about 40 nm, these modes can couple together, forming relatively narrow optical features. We showed that the lattice edge-mode quadrupole coupling was perpendicular to the polarization axis of the incident light. Therefore, the array of nanodisks supports a plasmonic lattice structure wherein along the *x*-axis the FNDs were coupled via near-plamonic fields, while along the *y*-axis they were coupled via their quadrupole modes.

Data availability statement

All data that support the findings of this study are included within the article (and any supplementary files).

Acknowledgment

This work is supported by US National Science Foundation under Grant No. ECCS-1917544.

ORCID iDs

Seyed M Sadeghi https://orcid.org/0000-0002-5043-5032 Waylin J Wing https://orcid.org/0000-0002-7104-5762

References

[1] Maier S A, Brongersma M L, Kik P G, Meltzer S, Requicha A A and Atwater H A 2001 Adv. Mater. 13 1501

[2] Dragoman M and Dragoman D 2008 Prog. Quantum Electron. 32 1

- [3] Ding F, Wang Z, He S, Shalaev V M and Kildishev A V 2015 ACS Nano 9 4111
- [4] Leroux Y, Lacroix J C, Fave C, Stockhausen V, Félidj N, Grand J, Hohenau A and Krenn J R 2009 Nano Lett. 9 2144
- [5] Gutha R R, Sadeghi S M, Sharp C and Wing W J 2017 Nanotechnology 28 355504
- [6] Chang W-S, Lassiter J B, Swanglap P, Sobhani H, Khatua S, Nordlander P, Halas N J and Link S 2012 Nano Lett. 12 4977
- [7] Hao F, Larsson E M, Ali T A, Sutherland D S and Nordlander P 2008 Chem. Phys. Lett. 458 262
- [8] Liu N, Langguth L, Weiss T, Kästel J, Fleischhauer M, Pfau T and Giessen H 2009 Nat. Mater. 8 758
- [9] Sakai K, Nomura K, Yamamoto T and Sasaki K 2015 Sci. Rep. 5 8431
- [10] Sakai K, Nomura K, Yamamoto T, Omura T and Sasaki K 2016 Sci. Rep. 6 34967
- [11] Kravets V G, Kabashin A V, Barnes W L and Grigorenko A N 2018 Chem. Rev. 118 5912
- [12] Rodriguez S R K, Abass A, Maes B, Janssen O T, Vecchi G and Rivas J G 2011 Phys. Rev. X 1 021019
- [13] Gutha R R, Sadeghi S M, Sharp C, Hatef A and Lin Y 2019 J. Appl. Phys. 125 023103
- [14] Bellido E P, Manjavacas A, Zhang Y, Cao Y, Nordlander P and Botton G A 2016 ACS Photonics 3 428
- [15] Campos A, Arbouet A, Martin J, Gerard D, Proust J, Plain J and Kociak M 2017 ACS Photonics 4 1257
- [16] Bellido E P, Zhang Y, Manjavacas A, Nordlander P and Botton G A 2017 ACS Photonics 4 1558–65
- [17] Schmidt F-P, Ditlbacher H, Hohenau A, Hohenester U, Hofer F and Krenn J R 2016 *Nano Lett.* **16** 5152
- [18] Schmidt F-P, Ditlbacher H, Hohenester U, Hohenau A, Hofer F and Krenn J R 2014 Nat. Commun. 5 3604

- [19] Sadeghi S M, Wing W J, Gutha R R, Sharp C and Hatef A 2017 J. Appl. Phys. 122 063102
- [20] Sadeghi S M, Dagallier A, Hatef A and Meunier M 2016 JOSA B 33 1502
- [21] Sadeghi S M, Gutha R R, Wing W J, Sharp C, Capps L and Mao C 2017 J. Phys. D: Appl. Phys. 50 145401
- [22] Gutha R R, Sadeghi S M, Hatef A, Sharp C and Lin Y 2018 Appl. Phys. Lett. 112 223102
- [23] Sadeghi S M, Gutha R R and Hatef A 2019 J. Opt. 21 035001
- [24] Keast V J, Walhout C, Pedersen T, Shahcheraghi N, Cortie M and Mitchell D R 2016 Plasmonics 11 1081
- [25] Imaeda K, Hasegawa S and Imura K 2018 J. Phys. Chem. C 122 7399
- [26] Bellido E P, Bernasconi G D, Rossouw D, Butet J, Martin O J and Botton G A 2017 ACS Nano 11 11240
- [27] Bicket I C, Bellido E P, McRae D M, Lagugné-Labarthet F and Botton G A 2020 ACS Photonics 7 1246
- [28] Lu X et al 2018 Nano Lett. 18 2879
- [29] El-Demellawi J K, Lopatin S, Yin J, Mohammed O F and Alshareef H N 2018 ACS Nano 12 8485
- [30] Sadeghi S M, Gutha R R and Hatef A 2019 Opt. Commun. 444 93
- [31] Sadeghi S M, Wing W J and Campbell Q 2016 J. Appl. Phys. 119 244503
- [32] Sadeghi S M, Wing W and Campbell Q 2016 *J. Appl. Phys.* **119** 114307
- [33] Esteban R, Aguirregabiria G, Borisov A G, Wang Y M, Nordlander P, Bryant G W and Aizpurua J 2015 ACS Photonics 2 295
- [34] Berthelot J, Bachelier G, Song M, Rai P, Des Francs G C, Dereux A and Bouhelier A 2012 Opt. Express 20 10498
- [35] Schmidt F-P, Losquin A, Hofer F, Hohenau A, Krenn J R and Kociak M 2017 ACS Photonics 5 861